Ultrasensitive and high gain solution-processed perovskite photodetectors by CH<sub>3</sub>NH<sub>3</sub>PbI<sub>2.55</sub>Br<sub>0.45</sub>:Zn<sub>2</sub>SnO<sub>4</sub> bulk heterojunction composite

Luyao Zheng, Wenzhan Xu, Xiang Yao, Tao Zhu, Yongrui Yang, Lei Liu & Xiong Gong

**Emergent Materials** 

ISSN 2522-5731

emergent mater. DOI 10.1007/s42247-020-00072-7





Your article is protected by copyright and all rights are held exclusively by Qatar **University and Springer Nature Switzerland** AG. This e-offprint is for personal use only and shall not be self-archived in electronic repositories. If you wish to self-archive your article, please use the accepted manuscript version for posting on your own website. You may further deposit the accepted manuscript version in any repository, provided it is only made publicly available 12 months after official publication or later and provided acknowledgement is given to the original source of publication and a link is inserted to the published article on Springer's website. The link must be accompanied by the following text: "The final publication is available at link.springer.com".



Emergent Materials https://doi.org/10.1007/s42247-020-00072-7

### **ORIGINAL ARTICLE**



# Ultrasensitive and high gain solution-processed perovskite photodetectors by CH<sub>3</sub>NH<sub>3</sub>Pbl<sub>2.55</sub>Br<sub>0.45</sub>:Zn<sub>2</sub>SnO<sub>4</sub> bulk heterojunction composite

Luyao Zheng 1 · Wenzhan Xu 1 · Xiang Yao 2 · Tao Zhu 1 · Yongrui Yang 1 · Lei Liu 1 · Xiong Gong 1

Received: 25 November 2019 / Accepted: 3 February 2020 © Qatar University and Springer Nature Switzerland AG 2020

### Abstract

Hybrid perovskite photodetectors, the novel alternative devices transform incident light into electrical signal, have been rapidly developed in the past years. However, intrinsic unbalanced charge carrier transport within hybrid perovskite materials, restricting further boosting device performance of perovskite photodetectors, has rarely been addressed. In this study, we report room temperature—operated solution-processed bulk heterojunction perovskite photodetectors with ultrahigh sensitivity and great photo-gain. It is found that the introduction of  $Zn_2SnO_4$  nanoparticles into  $CH_3NH_3PbI_{2.55}Br_{0.45}$  perovskites results in enlarged photocurrent and suppressed dark current for bulk heterojunction perovskite photodetectors. As a result, a responsivity of over  $1500 \text{ mAW}^{-1}$  and projected detectivity of approximatively  $10^{14} \text{ Jones}$  (1 Jones = cm  $\text{Hz}^{1/2} \text{ W}^{-1}$ ) from 380 to 760 nm are observed from bulk heterojunction perovskite photodetectors exhibit an excellent linear dynamic range of 124 dB and a great photo-gain of 535. All these results indicate that high-performance perovskite photodetectors could be realized through novel bulk heterojunction device structure.

**Keywords** Perovskite photodetectors · Zn<sub>2</sub>SnO<sub>4</sub> nanoparticles · High gain · High responsivity and detectivity

# 1 Introduction

Photodetectors (PDs) that transform incident light into electrical signal show great potential applications of light-signal detection including environmental monitoring, medical sensing, optical fiber communication, day and night surveillance, and light imaging [1–5]. Nowadays, various inorganic and organic

Luyao Zheng, Wenzhan Xu and Xiang Yao contributed equally to this work

**Electronic supplementary material** The online version of this article (https://doi.org/10.1007/s42247-020-00072-7) contains supplementary material, which is available to authorized users.

Published online: 03 March 2020

- Department of Polymer Engineering, College of Polymer Science and Polymer Engineering, The University of Akron, Akron, OH 44325, USA
- Institute of Molecular Plus, and Tianjin Key Laboratory of Molecular Optoelectronic Sciences, School of Science, Tianjin University and Collaborative Innovation Centre of Chemical Science and Engineering, Tianjin 300072, People's Republic of China

semiconductors have been greatly developed for fabrication of PDs. However, the high cost of inorganic-based PDs and their requirements to be operated at low temperature and high voltage for receiving reasonable detectivities restricted their large applications [6, 7]. Organic-based PDs possess cost-effective processability and room-temperature operational feature, but most of them exhibit low sensitivity due to inefficient charge transfer and low charge carrier mobilities, and poor stability owing to intrinsic instability of organic semiconductors [8–13].

Recently, organic-inorganic hybrid halide perovskites have been demonstrated to be the photoactive layer for photovoltaics (solar cells and photodetectors) due to its superior optoelectronic properties and solution processability [14–19]. In 2014, Dou et al. reported solution-processed perovskite PDs with an inverted device structure [20]. In 2015, we reported high-performance solution-processed perovskite PDs with a conventional device structure [21]. Recently, ultraviolet (UV)-visible to near-infrared (NIR) photoresponsivity from perovskite PDs, where perovskite materials were incorporated with either low-bandgap conjugated polymers or inorganic quantum dots (QDs), was reported [16, 22–24]. For example, by forming the double-layer structure of CH<sub>3</sub>NH<sub>3</sub>PbI<sub>3</sub>/NDI-









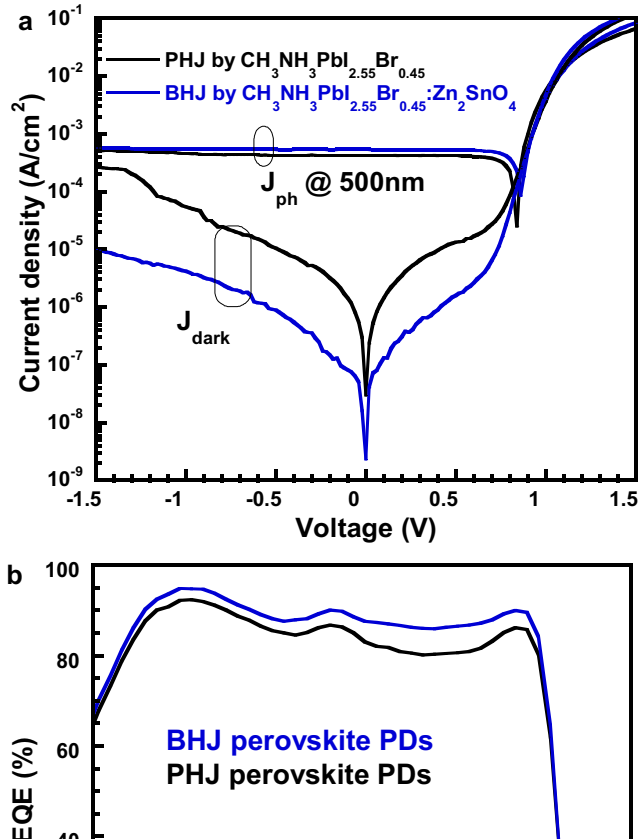
DPP (where NDI-DPP is poly[(N, N'-bis(2-octyldodecyl)-1,4,5,8-naphthalene diimide-2,6-diyl) (2,5-dioctyl-3,6di(thiophen-2-yl)pyrrolo [3,4-c]pyrrole-1,4-dione-5,5'-diyl)], an n-type narrow bandgap conjugated polymer) as the photoactive layer, solution-processed perovskite PDs with responsivity (R) of 150 mA W<sup>-1</sup> and projected detectivity  $(D^*)$  over  $10^{12}$  Jones (1 Jones = cm  $Hz^{1/2}$  W<sup>-1</sup>) in the NIR region were observed [16]. Perovskite PDs have been rapidly developed [20-26]; however, intrinsic unbalanced charge carrier transport within perovskite materials [27, 28], which restricts further boosting device performance of perovskite PDs, has not been fully addressed so far. In order to address unbalanced charge carrier transport within perovskite materials, bulk heterojunction (BHJ) device structure was firstly reported in our group for approaching efficient perovskite solar cells (PSCs) [29, 30]. As alternatives to construct BHJ composite with perovskite, metal oxide nanoparticles (NPs) exhibit unique optoelectrical properties [31–40]. More recently, we reported high-performance PSCs, where perovskite materials were incorporated with n-type Zn<sub>2</sub>SnO<sub>4</sub> NPs, which possess superior charge carrier mobility, as the photoactive layer [41].

In this study, we report a simple and versatile solution method for approaching ultrasensitive solution-processed perovskite PDs with BHJ device structure. Operated at room temperature, it is found that BHJ perovskite PDs exhibit a responsivity of over 1500 mAW<sup>-1</sup> and projected detectivity of approximatively 10<sup>14</sup> Jones from 380 to 760 nm. In addition, BHJ perovskite PDs possess excellent linear dynamic range of 124 dB and a great photo-gain of 535.

## 2 Results and discussion

Perovskite PDs with a BHJ device structure of ITO/PTAA/ CH<sub>3</sub>NH<sub>3</sub>PbI<sub>2.55</sub>Br<sub>0.45</sub>:Zn<sub>2</sub>SnO<sub>4</sub>/PC<sub>61</sub>BM/Al, and a planar heterojunction (PHJ) device structure of ITO/PTAA/ CH<sub>3</sub>NH<sub>3</sub>PbI<sub>2,55</sub>Br<sub>0,45</sub>/PC<sub>61</sub>BM/Al, where ITO is indium tin oxide, PTAA is polytriarylamine and acts as the hole extraction layer (HEL), PC<sub>61</sub>BM is [6,6]-phenyl-C61-butyric acid methyl ester and acts as the electron extraction layer (EEL), and Al is aluminum, respectively, were fabricated and characterized. The device structures for perovskite PDs under this study are the same as the device structures for PSCs reported previously [41]. Based on the band alignment of the materials and the electrodes used for fabrication BHJ perovskite PDs [41], the PTAA HEL is favorable for holes being extracted from CH<sub>3</sub>NH<sub>3</sub>PbI<sub>2.55</sub>Br<sub>0.45</sub>:Zn<sub>2</sub>SnO<sub>4</sub> BHJ composite to the ITO anode, which enhances the photocurrent density. The conduction band of Zn<sub>2</sub>SnO<sub>4</sub> NPs is -4.10 eV, which is located at between the lowest unoccupied molecular orbit (LUMO) energy level (-3.79-3.93 eV) of CH<sub>3</sub>NH<sub>3</sub>PbI<sub>2.55</sub>Br<sub>0.45</sub> and the LUMO energy (-4.20 eV) of the PC<sub>61</sub>BM EEL, forming the gradient energy level difference, and further reducing the direct energy loss. Owing to the deep valence band maximum (–7.90 eV) of Zn<sub>2</sub>SnO<sub>4</sub> NPs, it markedly increases the hole injection barrier between the Al cathode and CH<sub>3</sub>NH<sub>3</sub>PbI<sub>2.55</sub>Br<sub>0.45</sub>:Zn<sub>2</sub>SnO<sub>4</sub> BHJ composite from 1.20 to 3.60 eV, which is more efficient to block holes being injected into CH<sub>3</sub>NH<sub>3</sub>PbI<sub>2.55</sub>Br<sub>0.45</sub>:Zn<sub>2</sub>SnO<sub>4</sub> BHJ composite in dark from the external circuit, and thus, reduced dark current density is expected. Therefore, boosted photocurrent density and suppressed dark current density are expected to be observed from perovskite PDs with a BHJ device structure.

Operated at room temperature, the current density versus voltage (J-V) characteristics of perovskite PDs with either BHJ or PHJ device structures measured in dark and under a monochromatic light of 500 nm with a light intensity of 0.28 mW/cm<sup>2</sup> are shown in Fig. 1a. It is obvious that perovskite PDs with a BHJ device structure exhibit dramatically reduced dark current density at reverse bias compared with



40 500 600 700 800
Wavelength (nm)

Fig. 1 a The J-V characteristics and b EQE spectra of both BHJ and PHJ perovskite photodetectors







جامعة قطر

those from perovskite PDs with a PHJ device structure, i.e., biased at -0.5 V; a dark current density of  $8.97 \times 10^{-7}$  A cm<sup>-2</sup> observed from BHJ perovskite PDs is much smaller than that of  $1.05 \times 10^{-5}$  A cm<sup>-2</sup> observed from PHJ perovskite PDs, indicating the small amount of Zn<sub>2</sub>SnO<sub>4</sub> NPs would suppress leakage current. Such suppressed dark current density is attributed to the high-quality thin film morphology with diminished pinholes and grain boundaries of solution-processed CH<sub>3</sub>NH<sub>3</sub>PbI<sub>2</sub> <sub>55</sub>Br<sub>0</sub> <sub>45</sub>:Zn<sub>2</sub>SnO<sub>4</sub> BHJ composite thin film as compared with that of solution-processed pristine CH<sub>3</sub>NH<sub>3</sub>PbI<sub>2.55</sub>Br<sub>0.45</sub> thin film [41], and inhibition of charge injection from electrodes as discussed above. On the other hand, under monochromatic light of 500 nm, the photocurrent density of BHJ perovskite PDs is slightly higher than that from PHJ perovskite PDs, indicating that Zn<sub>2</sub>SnO<sub>4</sub> NPs is functionalized as the electron acceptor, boosting separated charge carrier to be efficiently transferred to the Al cathode [41]. Enhanced photocurrent and suppressed dark current indicate that BHJ perovskite PDs possess boosted detectivity [2].

The external quantum efficiency (EQE) spectra of both PHJ and BHJ perovskite PDs are shown in Fig. 1b. These EQE spectra are nearly the same as the EQE spectra of PSCs reported previously [41]. Both PHJ and BHJ perovskite PDs possess the identical photoresponse since  $Zn_2SnO_4$  NPs is a wide bandgap semiconductor and it has no contribution to the photocurrent over the wavelength ( $\lambda$ ) of 375 nm. However, as indicated in Fig. 1b, an enhancement in EQE is observed from 380 to 760 nm from BHJ perovskite PDs as compared with that of PHJ perovskite PDs, indicating that BHJ perovskite PDs generate more photocurrent than that of PHJ perovskite PDs. These observations are in good agreement with the J-V characteristics (Fig. 1a).

Thus, Zn<sub>2</sub>SnO<sub>4</sub> in the CH<sub>3</sub>NH<sub>3</sub>PbI<sub>2.55</sub>Br<sub>0.45</sub>:Zn<sub>2</sub>SnO<sub>4</sub> BHJ composite thin film plays two functionalities. Firstly, Zn<sub>2</sub>SnO<sub>4</sub> NPs serve as the electron acceptor to facilitate the charge carrier separation and transport in PDs under illumination. The n-type Zn<sub>2</sub>SnO<sub>4</sub> NPs and p-type perovskite could form p-n junction at the interface and benefit the separation of photogenerated electron-hole pairs, resulting in more extracted charge density as well as boosted electron mobility [41]. Thus, the boosted photocurrent is observed in PDs by CH<sub>3</sub>NH<sub>3</sub>PbI<sub>2 55</sub>Br<sub>0 45</sub>:Zn<sub>2</sub>SnO<sub>4</sub> BHJ composite thin film. Secondly, Zn<sub>2</sub>SnO<sub>4</sub> NPs act as nucleation center for the growth of perovskite crystal and help to improve the quality of resultant thin film with better uniformity, enlarged grain size, and suppressed pinholes and grain boundaries [41]. Such optimal thin film morphology delivers the reduced dark current in corresponding PDs.

Responsivity (R), one of the most important parameters for evaluating PDs performance, is described as [2, 42]:

$$R = \frac{J_{\rm ph}}{L_{\rm light}} \text{ or } R = \text{EQE} \times \frac{e}{hv} = \text{EQE} \times \frac{\lambda}{1240} \tag{1}$$

where  $J_{\rm ph}$  is photocurrent density,  $L_{\rm light}$  is the light intensity, e is the elementary charge, h is the Planck's constant,  $\nu$  is the frequency of optical signal, and  $\lambda$  is wavelength. Thus, biased at -0.5 V and under illumination at 500 nm with the light intensity of 0.28 mW/cm², the estimated R of 1632 mA/W is for PHJ perovskite PDs, whereas R of 1847 mA/W is for BHJ perovskite PDs.

Detectivity is another most important parameter for evaluating PD performance [2, 28]. Detectivity is dependent on the noise current, which includes shot noise, Johnson noise, and thermal fluctuation "flicker" noise [2, 42, 43]. If only, take the shot noise from the dark current density  $(J_d)$  into consideration, the projected detectivity  $(D^*)$  is described by [2]:

$$D^* = \frac{\text{EQE} \cdot \lambda}{1240\sqrt{2eJ_d}} = \frac{R}{\sqrt{2eJ_d}}$$
 (2)

Thus, biased at -0.5 V and under  $\lambda$  of 500 nm,  $D^*$  of  $9.09 \times 10^{12}$  Jones is estimated for PHJ perovskite PDs. Under the exact conditions,  $D^*$  of  $6.08 \times 10^{13}$  Jones is estimated for BHJ perovskite PDs, which is one of the highest value of PDs based on perovskite materials as listed in Table S1 [19, 21, 23, 44–48].

Based on Eqs. (1) and (2) and the EQE spectra of perovskite PDs (Fig. 1b), R and  $D^*$  versus wavelength for both BHJ and PHJ perovskite PDs could be estimated and the results are shown in Fig. 2. As compared with PHJ perovskite PDs, the enlarged R observed from BHJ perovskite PDs is attributed to boosted  $J_{\rm ph}$  due to photoinduced charge transfer among CH<sub>3</sub>NH<sub>3</sub>PbI<sub>2.55</sub>Br<sub>0.45</sub>:Zn<sub>2</sub>SnO<sub>4</sub> BHJ composite thin film [41]; the enhanced  $D^*$  observed from BHJ perovskite PDs is attributed to boosted  $J_{\rm ph}$  and suppressed  $J_{\rm d}$  as well. The suppressed  $J_{\rm d}$  is originated from superior film morphology induced by introduction the additional Zn<sub>2</sub>SnO<sub>4</sub> into CH<sub>3</sub>NH<sub>3</sub>PbI<sub>2.55</sub>Br<sub>0.45</sub> thin film [41]. Overall, BHJ perovskite PDs with average R of over 1500 mA/W and  $D^*$  of

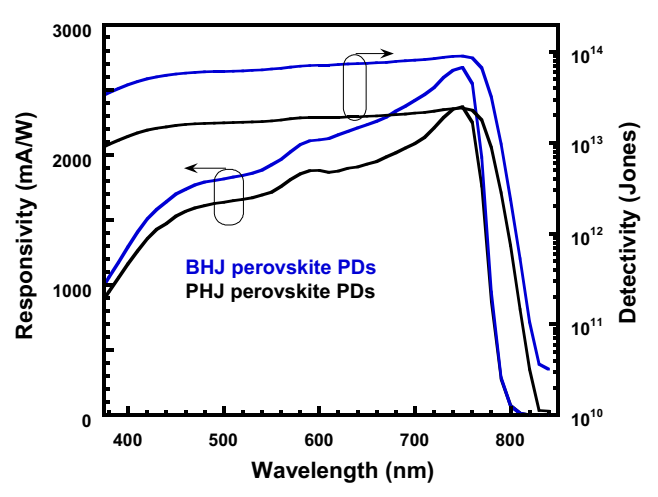


Fig. 2 Responsivity and detectivity versus wavelength for both BHJ and PHJ perovskite photodetectors









approximatively  $10^{14}$  Jones are observed in  $\lambda$  ranging from 375 to 760 nm. These device performance parameters are compatible to those Si-based PDs operated at low temperature [49–51].

Linear dynamic region (LDR) is a crucial figure of merit for evaluating PDs. The LDR (typically quoted in dB) is described as [2]:

$$LDR = 20 \log \frac{J_{\text{ph}}^*}{J_{\text{d}}} \tag{3}$$

where  $J_{\rm ph}^*$  is the photocurrent density measured at the light intensity of 1 mW/cm<sup>2</sup>. Figure 3 shows the photocurrent densities versus the light intensities for both PHJ and BHJ perovskite PDs. The LDR for PHJ perovskite PDs is 108 dB, whereas the LDR for BHJ perovskite PDs is 124 dB. Such high LDR is one of the highest values among the reported perovskite PDs [20, 52–55]. Moreover, this value is comparable with commercial Si PDs (120 dB) and higher than other types of PDs such as organic PDs [56, 57].

Fast and reliable responses to light illumination are important to high-performance PDs [42, 43]. The response times, which include rising response to light on and decaying response to light off, are strongly related to the charge transport and collection and describe how sensitive of the PDs towards light

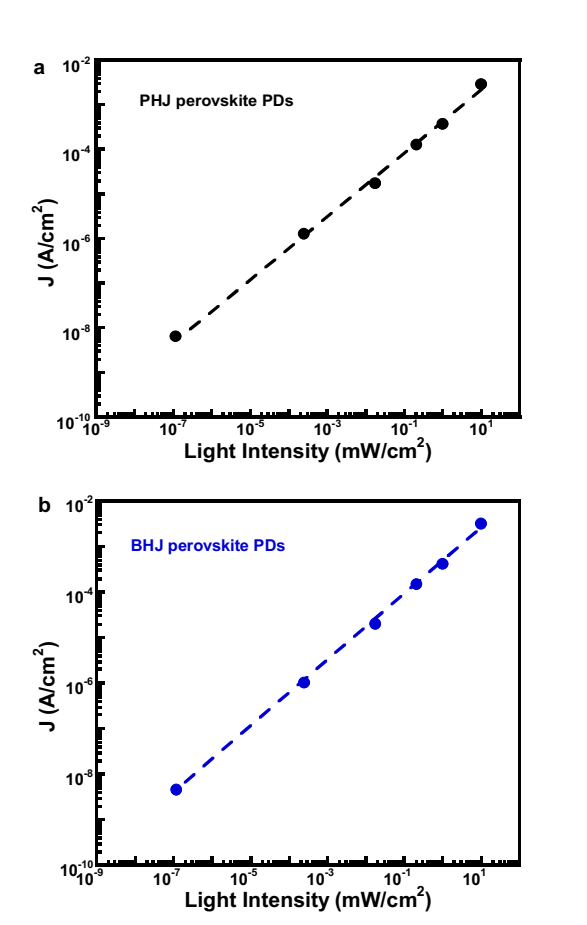


Fig. 3 The photocurrent densities versus the light intensities for  $a\ \mathrm{PHJ}$  and  $b\ \mathrm{BHJ}$  perovskite photodetectors







جاممة قطر 📗

switching on and off. The temporal response of the photocurrent of perovskite PDs is characterized by using an optical chopper controlled at  $\lambda = 532$ -nm laser pulse at a frequency of 1 kHz. The rise time and decay time are defined as the time required for output signals to increase from 10 to 90% of the peak photocurrent and decrease from 90 to 10% of the peak photocurrent [22]. Figure 4 displays the transient photocurrent of both PHJ and BHJ perovskite PDs. The rise times of 11.9 us and 4.2 µs are observed from PHJ perovskite PDs and BHJ perovskite PDs, respectively. However, a biexponential photocurrent decay with time constant of 10.4 µs for PHJ perovskite PDs is obtained. In contrast, BHJ perovskite PDs exhibit longer decay time of 3.2 µs. The faster rise time and decay time in PDs by BHJ perovskite illustrate the sensitive response to light switching owing to the improved charge transport and facile charge collection after incorporating with Zn<sub>2</sub>SnO<sub>4</sub> NPs.

The photo-gain (PG) of PDs is determined by the ratio recombination lifetime ( $\tau_{life}$ ) to charge transmit time ( $\tau_{transit}$ ), given by [58, 59]:

$$PG = \frac{\tau_{life}}{\tau_{transit}} = \frac{\tau_{life}}{d^2/\mu V}$$
 (4)

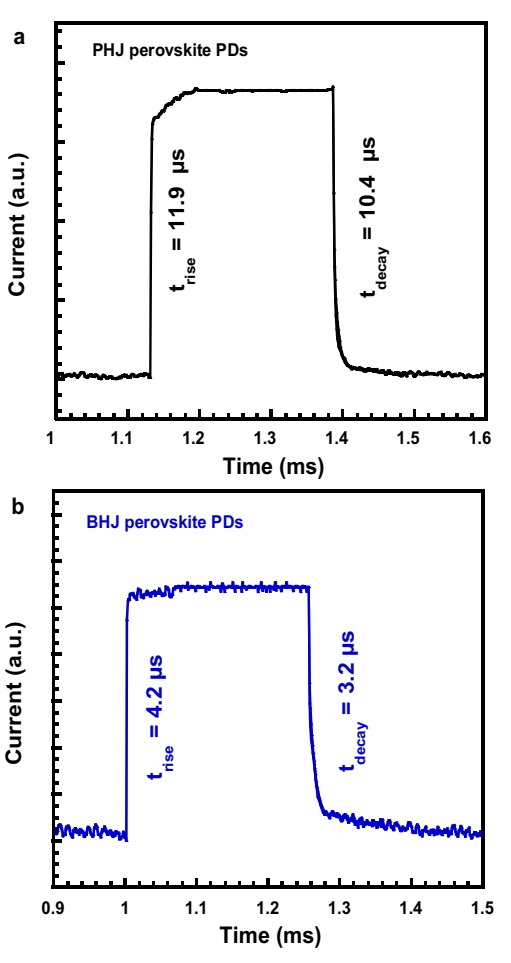


Fig. 4 The transient photocurrent of a PHJ and b BHJ perovskite photodetectors

where d is the thickness of perovskite thin film,  $\mu$  is the charge carrier mobility, and V is the applied bias. For PHJ perovskite PDs, at V=0.5 V and d=340 nm, the charge carrier recombination lifetime is estimated to be 8.1  $\mu$ s, and the hole mobility is estimated to be  $1.16 \times 10^{-2}$  cm<sup>2</sup> V<sup>-1</sup> s<sup>-1</sup> [41]. For BHJ perovskite PDs, at V=0.5 V and d=360 nm, the charge carrier recombination lifetime is estimated to be 1.8  $\mu$ s, and the hole mobility is estimated to be 1.8  $\mu$ s, and the hole mobility is estimated to be 1.8  $\mu$ s, and 1.8 Thus, the estimated PG values are 43 and 535 for PHJ perovskite PDs and BHJ perovskite PDs, respectively. These results demonstrate that BHJ perovskite PDs could get more PG as compared with that of PHJ perovskite PDs.

In summary, we reported room temperature-operated solution-processed bulk heterojunction (BHJ) perovskite photodetectors (PDs) by CH<sub>3</sub>NH<sub>3</sub>PbI<sub>2.55</sub>Br<sub>0.45</sub> blended with Zn<sub>2</sub>SnO<sub>4</sub> NPs. Zn<sub>2</sub>SnO<sub>4</sub> NPs acted as the electron acceptors for boosting photocurrent in BHJ perovskite PDs. Zn<sub>2</sub>SnO<sub>4</sub> NPs also promotes the formation of high-quality perovskite thin film and generates photoinduced charge transfer, resulting in enlarged photocurrent and suppressed dark current for BHJ perovskite PDs. A responsivity of over 1500 mAW<sup>-1</sup> and projected detectivity of approximatively 10<sup>14</sup> Jones from 380 to 760 nm, which are compatible to Si-based PDs and higher than those from other perovskite PDs, were observed from BHJ perovskite PDs. In addition, BHJ perovskite PDs exhibit excellent linear dynamic range of 124 dB and great photo-gain of 535. All these device performance parameters are better than those of perovskite PDs with a planar heterojunction device structure. Our discovery reported in this study demonstrates that fabrication of BHJ perovskite PDs is an appropriate approach to realize high-performance perovskite PDs.

# 3 Experimental

Materials Lead iodide (PbI<sub>2</sub>, 99.999%), poly(triaryl amine) (PTAA), methylammonium bromide (MABr), anhydrous N,N-dimethylformamide (DMF, 99.8%), anhydrous ethanol (>99.5%), anhydrous toluene (99.8%), anhydrous chlorobenzene (CB, 99.8%), zinc chloride (ZnCl<sub>2</sub>), tin (IV) chloride pentahydrate (SnCl<sub>4</sub>·5H<sub>2</sub>O), zinc acetate dehydrate, and all other reagents were purchased from Sigma-Aldrich and used as received without further purification. [6,6]-Phenyl-C61-butyric acid methyl ester (PC<sub>61</sub>BM, 99.5%) was purchased from Solenne BV and used as received without further purification. Methylammonium iodide (CH<sub>3</sub>NH<sub>3</sub>I (MAI)) was synthesized by using hydroiodic acid and methylamine in our laboratory.

Preparation of Zn<sub>2</sub>SnO<sub>4</sub> NPs The detailed preparation procedures are described in other literatures [41].

**Perovskite precursor preparation**  $PbI_2$  was dissolved into DMF solvent with a concentration of 400 mg mL<sup>-1</sup>, followed by magnetically stirred at 70 °C for ~12 hours (h) until the cloudy solution yields to transparent yellow solution. For BHJ perovskite PDs fabricated by  $CH_3NH_3PbI_{2.55}Br_{0.45}:Zn_2SnO_4$  thin film,  $PbI_2$  was dissolved in mix solution of  $Zn_2SnO_4$  DMF solution where DMF is with a concentration of 400 mg mL<sup>-1</sup>. Mixture MAI:MABr (85:15 by molar ratio) was dissolved into ethanol solvent to make a concentration of total 35 mg mL<sup>-1</sup> solutions.

Fabrication of perovskite photodetectors Approximately 8-nm PTAA layer is spin-coated onto pre-cleaned and UV-Ozonetreated ITO-coated glass substrates from PTAA toluene solution with the concentration of 2 mg mL<sup>-1</sup> at 6000 RPM for 40 seconds (s), followed with thermal annealing at 100 °C for 10 min (min) on the hotplate in the glovebox with a nitrogen atmosphere. PbI<sub>2</sub> layer is spin-casted on the top of the pre-heated (85 °C) ITO/PTAA substrates from the warmed (85 °C) PbI<sub>2</sub> solution at a spin speed of 6000 RPM for 20 s with an acceleration time of 5 s, followed with thermal annealing at 85 °C for 10 min on the hotplate, and then cooling down to room temperature. Afterward, the mixture MAI:MABr solution is spin-coated on the top of PbI<sub>2</sub> layer at a spin speed of 6000 RPM for 40 s with an acceleration time of 5 s, followed by thermal annealing at 100 °C for 2 h on the hotplate to form CH<sub>3</sub>NH<sub>3</sub>PbI<sub>2 55</sub>Br<sub>0 45</sub> thin film. For CH<sub>3</sub>NH<sub>3</sub>PbI<sub>2.55</sub>Br<sub>0.45</sub>:Zn<sub>2</sub>SnO<sub>4</sub> thin film, PbI<sub>2</sub> is mixed with Zn<sub>2</sub>SnO<sub>4</sub> DMF solution. The thickness of CH<sub>3</sub>NH<sub>3</sub>PbI<sub>2,55</sub>Br<sub>0,45</sub> and CH<sub>3</sub>NH<sub>3</sub>PbI<sub>2,55</sub>Br<sub>0,45</sub>:Zn<sub>2</sub>SnO<sub>4</sub> thin films are measured to be  $\sim 340$  nm and  $\sim 360$  nm, respectively. After the perovskite layer was cooled down to room temperature,  $\sim$  60 nm PC<sub>61</sub>BM is spin-coated on the top of perovskite layer at a spin speed of 1800 RPM for 30 s with an acceleration time of 2 s from the PC<sub>61</sub>BM chlorobenzene solution with the concentration of 20 mg mL<sup>-1</sup>. Lastly, a 100-nm-thick Al is thermally deposited through a shadow mask in the vacuum with the press of  $4 \times 10^{-6}$  mbar. The active device area is measured to be  $0.045 \text{ cm}^2$ .

Characterization of perovskite photodetectors The J-V characteristics of perovskite PDs were measured in dark and under monochromatic light of 500 nm with a light intensity of 0.28 mW/cm² from a Xenon lamp on a Keithley model 2400 source measure unit. The EQE is obtained by using the solar cell quantum efficiency measurement system (QEX10) from PV measurements with a 300-W steady-state xenon lamp as the source light. The transient photocurrent measurements were performed by using an optical chopper controlled at  $\lambda = 532\text{-nm}$  laser pulse at a frequency of 2 kHz.

**Acknowledgments** The authors received financial support from the University of Akron thank National Science Foundation (EECs 1351785 and EECs 1903303).









# Compliance with ethical standards

**Conflict of interest** The authors declare that they have no conflict of interest.

# References

- X. Wang, Z. Cheng, K. Xu, H.K. Tsang, J.-B. Xu, Highresponsivity graphene/silicon-heterostructure waveguide photodetectors, Nat. Photonics 7(11), 888–891 (2003)
- X. Gong, M. Tong, Y. Xia, W. Cai, J.S. Moon, Y. Cao, G. Yu, S.L. Shieh, B. Nilsson, A.J. Heeger, High-detectivity polymer photodetectors with spectral response from 300 nm to 1450 nm. Science 325(5948), 1665–1667 (2009)
- J. Tafur, E.P. Van Wijk, R. Van Wijk, P.J. Mills, Biophoton detection and low-intensity light therapy: a potential clinical partnership. Photomed. Laser Surg. 28(1), 23–30 (2010)
- T. Mueller, F. Xia, P. Avouris, Graphene photodetectors for highspeed optical communications. Nat. Photonics 4(5), 297–301 (2010)
- Q. Lin, A. Armin, D.M. Lyons, P.L. Burn, P. Meredith, Low noise, IR-blind organohalide perovskite photodiodes for visible light detection and imaging. Adv. Mater. 27(12), 2060–2064 (2015)
- J. Michel, J. Liu, L.C. Kimerling, High-performance Ge-on-Si photodetectors. Nat. Photonics 4(8), 527–534 (2010)
- W. Wei, X.-Y. Bao, C. Soci, Y. Ding, Z.-L. Wang, D. Wang, Direct heteroepitaxy of vertical InAs nanowires on Si substrates for broad band photovoltaics and photodetection. Nano Lett. 9(8), 2926– 2934 (2009)
- W.-W. Tsai, Y.-C. Chao, E.-C. Chen, H.-W. Zan, H.-F. Meng, C.-S. Hsu, Increasing organic vertical carrier mobility for the application of high speed bilayered organic photodetector. Appl. Phys. Lett. 95(21), 306 (2009)
- Z. Liu, K. Parvez, R. Li, R. Dong, X. Feng, K. Müllen, Transparent conductive electrodes from graphene/PEDOT: PSS hybrid inks for ultrathin organic photodetectors. Adv. Mater. 27(4), 669–675 (2015)
- M. Kielar, M. Daanoune, O. François-Martin, B. Flament, O. Dhez, A.K. Pandey, S. Chambon, R. Clerc, L. Hirsch, Insights into the failure mechanisms of organic photodetectors. Adv. Electron. Mater 4(2), 1700526 (2018)
- W. Wang, F. Zhang, M. Du, L. Li, M. Zhang, K. Wang, Y. Wang, B. Hu, Y. Fang, J. Huang, Highly narrowband photomultiplication type organic photodetectors. Nano Lett. 17(3), 1995–2002 (2017)
- Z. Zhao, J. Wang, C. Xu, K. Yang, F. Zhao, K. Wang, X.L. Zhang, F. Zhang, Photomultiplication type broad response organic photodetectors with one absorber layer and one multiplication layer. J. Phys. Chem. Lett. 11(2), 366–373 (2020)
- J. Miao, F. Zhang, Recent progress on photomultiplication type organic photodetectors. Laser Photonics Rev. 13, 1800204 (2019)
- M.M. Lee, J. Teuscher, T. Miyasaka, T.N. Murakami, H.J. Snaith, Efficient hybrid solar cells based on meso-superstructured organometal halide perovskites. Science 338(6107), 643–647 (2012)
- C. Wehrenfennig, G.E. Eperon, M.B. Johnston, H.J. Snaith, L.M. Herz, High charge carrier mobilities and lifetimes in organolead trihalide perovskites. Adv. Mater. 26(10), 1584–1589 (2014)
- W. Xu, Y. Guo, X. Zhang, L. Zheng, T. Zhu, D. Zhao, W. Hu, X. Gong, Room-temperature-operated ultrasensitive broadband photo-detectors by perovskite incorporated with conjugated polymer and single-wall carbon nanotubes. Adv. Funct. Mater. 28(7), 1705541 (2018)







- Y. Guo, C. Liu, H. Tanaka, E. Nakamura, Air-stable and solutionprocessable perovskite photodetectors for solar-blind UV and visible light. J. Phys. Chem. Lett. 6(3), 535–539 (2015)
- M. Liu, M.B. Johnston, H.J. Snaith, Efficient planar heterojunction perovskite solar cells by vapour deposition. Nature 501(7467), 395–398 (2013)
- S. Chen, C. Teng, M. Zhang, Y. Li, D. Xie, G. Shi, A flexible UV– Vis–NIR photodetector based on a perovskite/conjugated-polymer composite. Adv. Mater. 28(28), 5969–5974 (2016)
- L. Dou, Y.M. Yang, J. You, Z. Hong, W.-H. Chang, G. Li, Y. Yang, Solution-processed hybrid perovskite photodetectors with high detectivity. Nat. Commun. 5, 5404 (2014)
- C. Liu, K. Wang, C. Yi, X. Shi, P. Du, A.W. Smith, A. Karim, X. Gong, Ultrasensitive solution-processed perovskite hybrid photodetectors. J. Mater. Chem. C 3(26), 6600–6606 (2015)
- Y. Wang, D. Yang, X. Zhou, D. Ma, A. Vadim, T. Ahamad, S.M. Alshehri, Perovskite/polymer hybrid thin films for high external quantum efficiency photodetectors with wide spectral response from visible to near-infrared wavelengths. Adv. Opt. Mater. 5(12), 1700213 (2017)
- C. Liu, K. Wang, P. Du, E. Wang, X. Gong, A.J. Heeger, Ultrasensitive solution-processed broad-band photodetectors using CH<sub>3</sub>NH<sub>3</sub>PbI<sub>3</sub> perovskite hybrids and PbS quantum dots as light harvesters. Nanoscale 7(39), 16460–16469 (2015)
- J. Miao, F. Zhang, Recent progress on highly sensitive perovskite photodetectors. J. Mater. Chem. C 7(7), 1741–1791 (2019)
- H. Deng, X. Yang, D. Dong, B. Li, D. Yang, S. Yuan, K. Qiao, Y.-B. Cheng, J. Tang, H. Song, Flexible and semitransparent organolead triiodide perovskite network photodetector arrays with high stability. Nano Lett. 15(12), 7963–7969 (2015)
- K. Wang, C. Wu, D. Yang, Y. Jiang, S. Priya, Quasi-twodimensional halide perovskite single crystal photodetector. ACS Nano 12(5), 4919

  –4929 (2018)
- V.W. Bergmann, S.A. Weber, F.J. Ramos, M.K. Nazeeruddin, M. Grätzel, D. Li, A.L. Domanski, I. Lieberwirth, S. Ahmad, R. Berger, Real-space observation of unbalanced charge distribution inside a perovskite-sensitized solar cell. Nat. Commun. 5, 5001 (2014)
- G.A. Elbaz, D.B. Straus, O.E. Semonin, T.D. Hull, D.W. Paley, P. Kim, J.S. Owen, C.R. Kagan, X. Roy, Unbalanced hole and electron diffusion in lead bromide perovskites. Nano Lett. 17(3), 1727–1732 (2017)
- K. Wang, C. Liu, P. Du, J. Zheng, X. Gong, Bulk heterojunction perovskite hybrid solar cells with large fill factor. Energy Environ. Sci. 8(4), 1245–1255 (2015)
- C. Liu, K. Wang, P. Du, C. Yi, T. Meng, X. Gong, Efficient solution-processed bulk heterojunction perovskite hybrid solar cells. Adv. Energy Mater. 5(12), 1402024 (2015)
- D. Ponnamma, A. Erturk, H. Parangusan, K. Deshmukh, M.B. Ahamed, M.A.A. Al-Maadeed, Stretchable quaternary phasic PVDF-HFP nanocomposite films containing graphene-titania-SrTiO<sub>3</sub> for mechanical energy harvesting. Emergent Mater. 1(1–2), 55–65 (2018)
- K. Karthik, M.M. Naik, M. Shashank, M. Vinuth, V. Revathi, Microwave-assisted ZrO<sub>2</sub> nanoparticles and its photocatalytic and antibacterial studies. J. Clust. Sci. 30(2), 311–318 (2019)
- K. Karthik, M.P. Nikolova, A. Phuruangrat, S. Pushpa, V. Revathi, M. Subbulakshmi, Ultrasound-assisted synthesis of V<sub>2</sub>O<sub>5</sub> nanoparticles for photocatalytic and antibacterial studies. Mater. Res. Innov. 25, 1–6 (2019)
- K. Karthik, S. Vijayalakshmi, A. Phuruangrat, V. Revathi, U. Verma, Multifunctional applications of microwave-assisted biogenic TiO<sub>2</sub> nanoparticles. J. Clust. Sci. 30(4), 965–972 (2019)
- K. Karthik, M. Shashank, V. Revathi, T. Tatarchuk, Facile microwave-assisted green synthesis of NiO nanoparticles from Andrographis paniculata leaf extract and evaluation of their

- photocatalytic and anticancer activities. Mol. Cryst. Liq. Cryst. **673**(1), 70–80 (2018)
- K. Kannan, D. Radhika, A. Nesaraj, M. Wasee Ahmed, R. Namitha, Cost-effective method of Co-doped rare-earth-based ceria (Y-CGO) nanocomposite as electrolyte for LT-SOFCs using C-TAB as surfactant. Mater. Res. Innov. 25, 1–8 (2019)
- D. Radhika, K. Kannan, A. Neseraj, R. Namitha, Facile low-temperature synthesis and application of La<sub>0.85</sub>Sr<sub>0.15</sub>Co<sub>0.85</sub>Fe<sub>0.15</sub>O<sub>3.85</sub> as superior cathode for LT-SOFCs using C-TAB as surfactant. Mater. Res. Innov. 25, 1–7 (2019)
- K. Karthik, S. Dhanuskodi, C. Gobinath, S. Sivaramakrishnan, Microwave-assisted synthesis of CdO–ZnO nanocomposite and its antibacterial activity against human pathogens. Spectrochim. Acta A Mol. Biomol. Spectrosc. 139, 7–12 (2015)
- P. Nagaraju, R. Vasudevan, M. Arivanandhan, A. Alsalme, R. Jayavel, High-performance electrochemical capacitor based on cuprous oxide/graphene nanocomposite electrode material synthesized by microwave irradiation method. Emergent Mater. 2(4), 495–504 (2019)
- Y.G. Reddy, A. Awasthi, A.S. Chary, S.N. Reddy, Characterization and ion transport studies through impedance spectroscopy on (1x)Pb(NO<sub>3</sub>)<sub>2</sub>: xAl<sub>2</sub>O<sub>3</sub> composite solid electrolytes. Emergent Mater. 1(3–4), 175–184 (2018)
- W. Xu, L. Zheng, T. Zhu, L. Liu, X. Gong, Bulk heterojunction perovskite solar cells incorporated with Zn2SnO4 nanoparticles as the electron acceptors. ACS Appl. Mater. Interfaces 11(37), 34020– 34029 (2019)
- A. Jha, Infrared technology, applications to electro-optics, photonic devices, and sensors. Infrared 11, 1944–1948 (2000)
- 43. P. Bhattacharya, L.Y. Pang, Semiconductor optoelectronic devices (Prentice Hall, Upper Saddle River, 1997)
- Y. Fang, J. Huang, Resolving weak light of sub-picowatt per square centimeter by hybrid perovskite photodetectors enabled by noise reduction. Adv. Mater. 27(17), 2804–2810 (2015)
- M.I. Saidaminov, M.A. Haque, M. Savoie, A.L. Abdelhady, N. Cho, I. Dursun, U. Buttner, E. Alarousu, T. Wu, O.M. Bakr, Perovskite photodetectors operating in both narrowband and broadband regimes. Adv. Mater. 28(37), 8144

  –8149 (2016)
- V.Q. Dang, G.-S. Han, T.Q. Trung, Y.-U. Jin, B.-U. Hwang, H.-S. Jung, N.-E. Lee, Methylammonium lead iodide perovskitegraphene hybrid channels in flexible broadband phototransistors. Carbon 105, 353–361 (2016)
- H. Xia, S. Tong, C. Zhang, C. Wang, J. Sun, J. He, J. Zhang, Y. Gao, J. Yang, Flexible and air-stable perovskite network photodetectors based on CH3NH3PbI3/C8BTBT bulk heterojunction. Appl. Phys. Lett. 112(23), 233301 (2018)

- S. Tong, H. Wu, C. Zhang, S. Li, C. Wang, J. Shen, S. Xiao, J. He, J. Yang, J. Sun, Large-area and high-performance CH3NH3PbI3 perovskite photodetectors fabricated via doctor blading in ambient condition. Org. Electron. 49, 347–354 (2017)
- F. Guo, B. Yang, Y. Yuan, Z. Xiao, Q. Dong, Y. Bi, J. Huang, A nanocomposite ultraviolet photodetector based on interfacial trapcontrolled charge injection. Nat. Nanotechnol. 7(12), 798 (2012)
- X. Li, M. Zhu, M. Du, Z. Lv, L. Zhang, Y. Li, Y. Yang, T. Yang, X. Li, K. Wang, High detectivity graphene-silicon heterojunction photodetector. Small 12(5), 595–601 (2016)
- H. Zhang, X. Zhang, C. Liu, S.-T. Lee, J. Jie, High-responsivity, high-detectivity, ultrafast topological insulator Bi<sub>2</sub>Se<sub>3</sub>/silicon heterostructure broadband photodetectors. ACS Nano 10(5), 5113–5122 (2016)
- H.L. Zhu, J. Cheng, D. Zhang, C. Liang, C.J. Reckmeier, H. Huang, A.L. Rogach, W.C. Choy, Room-temperature solution-processed NiO<sub>x</sub>:PbI<sub>2</sub> nanocomposite structures for realizing highperformance perovskite photodetectors. ACS Nano 10(7), 6808– 6815 (2016)
- C. Liu, H. Peng, K. Wang, C. Wei, Z. Wang, X. Gong, PbS quantum dots-induced trap-assisted charge injection in perovskite photodetectors. Nano Energy 30, 27–35 (2016)
- L. Zheng, T. Zhu, W. Xu, J. Zheng, L. Liu, X. Gong, Ultrasensitive perovskite photodetectors by Co partially substituted hybrid perovskite. ACS Sustain. Chem. Eng. 6(9), 12055–12060 (2018)
- L. Zheng, K. Wang, T. Zhu, L. Liu, J. Zheng, X. Gong, Solutionprocessed ultrahigh detectivity photodetectors by hybrid perovskite incorporated with heterovalent neodymium cations. ACS Omega 4(14), 15873–15878 (2019)
- X. Hu, K. Wang, C. Liu, T. Meng, Y. Dong, S. Liu, F. Huang, X. Gong, Y. Cao, High-detectivity inverted near-infrared polymer photodetectors using cross-linkable conjugated polyfluorene as an electron extraction layer. J. Mater. Chem. C 2(45), 9592–9598 (2014)
- H.L. Zhu, W.C. Choy, W.E. Sha, X. Ren, Photovoltaic mode ultraviolet organic photodetectors with high on/off ratio and fast response. Adv. Opt. Mater. 2(11), 1082–1089 (2014)
- G. Konstantatos, M. Badioli, L. Gaudreau, J. Osmond, M. Bernechea, F.P.G. De Arquer, F. Gatti, F.H. Koppens, Hybrid graphene–quantum dot phototransistors with ultrahigh gain. Nat. Nanotechnol. 7(6), 363 (2012)
- F. Li, H. Wang, D. Kufer, L. Liang, W. Yu, E. Alarousu, C. Ma, Y. Li, Z. Liu, C. Liu, N. Wei, F. Wang, L. Chen, O.F. Mohammed, A. Fratalocchi, X. Liu, G. Konstantatos, T. Wu, Ultrahigh carrier mobility achieved in photoresponsive hybrid perovskite films via coupling with single-walled carbon nanotubes. Adv. Mater. 29(16), 1602432 (2017)





